Rodent Model of Experimental Autoimmune-Orchitis

Subjects: Endocrinology & Metabolism
Contributor: Fabian Hemm

The rodent model of experimental autoimmune-orchitis (EAO) was established to analyze the underlying mechanisms of male infertility and causes of reduced testosterone concentration.

Keywords: experimental autoimmune-orchitis ; osteoporosis ; mouse model ; biomechanical properties ; rodent model ; Complete Freund's Adjuvant ; Bordetella pertussis toxin

1. Introduction

Testicular inflammation is mainly caused by bacterial infections, either sexually transmitted or from the urinary tract, and often develops a chronic asymptomatic disease progression [1][2][3][4]. Therefore, orchitis can persist over prolonged periods until adequate therapy is started and may result in irreversible long-term damage regarding the reproductive system [2][3]. In this regard, inflammatory infiltrates in the testicular interstitium, damaged seminiferous tubules and disorder of spermatogenesis have been illustrated [2]. In most cases inflammation affects epididymides as well, and leads to a combined epididymo-orchitis [1][2]. Consequently, orchitis, or rather epididymo-orchitis, represents a frequent cause of fertility disorders in young men [3][5]. However, the majority of fertility disorders are diagnosed a long time after the initial inflammatory process. Thus, in vitro and in vivo models are crucial to investigate the underlying processes of epididymo-orchitis and its complications. In this context the rodent model of experimental autoimmune-orchitis (EAO) represents a well-established animal model to evaluate the processes of testicular inflammation, consequences regarding the reproductive functionality and possible therapy options [6][7][8][9]. Furthermore, EAO was found to significantly reduce the testosterone concentration in rats in a similar way to human orchitis [6]. Androgens are known to represent a major impact factor regarding bone metabolism in men [10][11][12]. Accordingly, human studies illustrated the development of osteoporosis even in young men suffering from hypogonadism [13][14].

2. Histomorphometric Bone Architecture

Microscopic overviews of hematoxylin-eosin-stained vertebral bodies (**Figure 1**) were automatically evaluated regarding bone area (B.Ar), trabecular thickness (Tb.Th) and trabecular separation (Tb.Sp), while the trabecular perimeter (Tb.Pm) was measured manually. Histomorphometrical measurement illustrated a significantly decreased bone area due to EAO (0.361 ± 0.020 mm^2) and nearly significant reduction in the adjuvant group (Adj; 0.453 ± 0.043 mm^2) compared to the control group (Cont; 0.594 ± 0.048 mm^2, $p < 0.01$ vs. EAO, $p = 0.080$ vs. Adj, **Figure 2**). However, trabecular perimeter (EAO 17.082 ± 1.190 mm, Adj 17.358 ± 0.658 mm, Cont 21.550 ± 2.274 mm), trabecular thickness (EAO 17.050 ± 1.942 µm, Adj 17.509 ± 0.904 µm, Cont 18.024 ± 0.971 µm) and trabecular separation (EAO 106.298 ± 12.552 µm, Adj 108.196 ± 3.266 µm, Cont 87.265 ± 6.338 µm) remained without significant alterations.

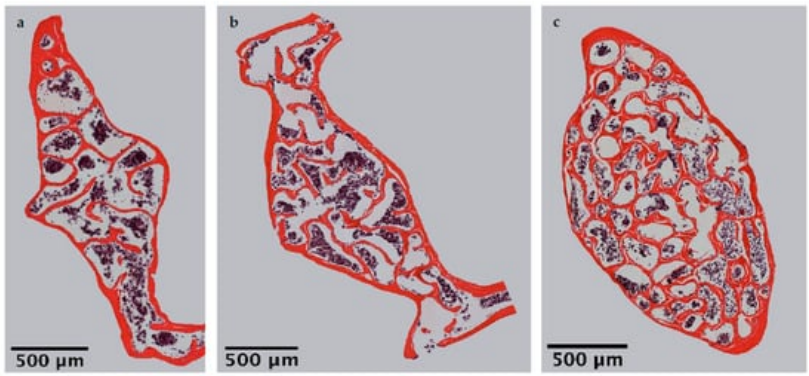

Figure 1. Microscopic overviews of vertebral bodies L3 stained with hematoxylin-eosin. Images taken at 40× magnification were merged. Mice were immunized with (**a**) testicular homogenate in adjuvant (EAO), (**b**) adjuvant alone or (**c**) remained untreated.

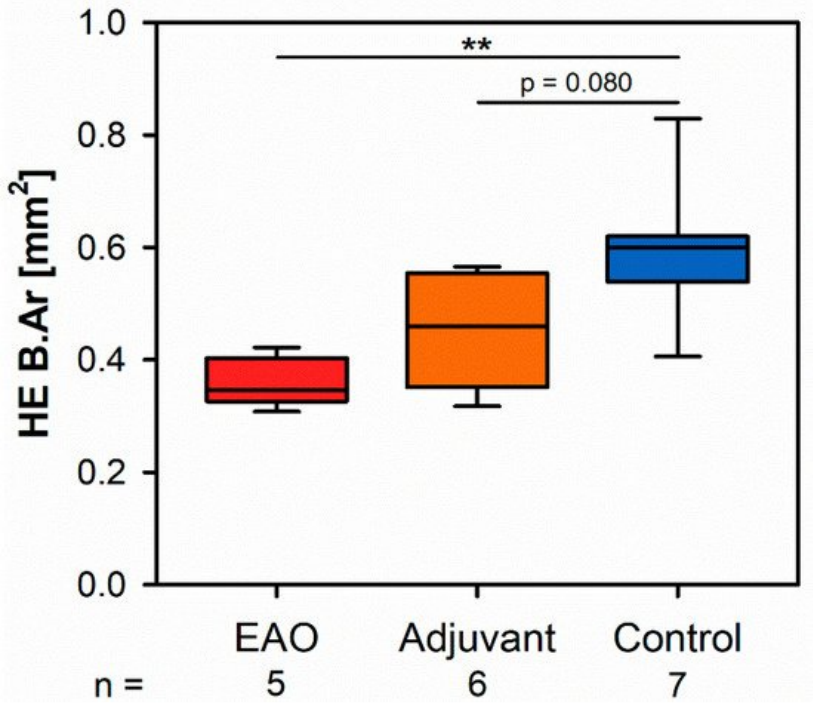

Figure 2. Histomorphometrical results regarding the bone area (B.Ar) in vertebral bodies L3 stained with hematoxylin-eosin (HE). Mice were immunized with testicular homogenate in adjuvant (EAO), adjuvant alone (adjuvant) or remained untreated (control). ** $p < 0.01$.

3. Microarchitecture of Cortical Bone

The microarchitecture of the femoral cortex was analyzed at mid diaphysis and distal diaphysis by micro computed tomography (µCT). Two-dimensional example images from µCT scans (**Figure 3**) demonstrated a loss of cortical as well as trabecular bone mass following (a) EAO or (b) treatment with adjuvant alone, compared to (c) untreated mice.

Figure 3. Two-dimensional images from µCT scans of distal femora (scale bar 2 mm). Mice were immunized with (**a**) testicular homogenate in adjuvant (EAO), (**b**) adjuvant alone or (**c**) remained untreated.

At the mid diaphyseal region, µCT identified a significantly reduced cortical thickness (Ct.Th, **Figure 4**a) in the EAO (0.147 ± 0.005 mm) and adjuvant group (0.155 ± 0.005 mm) in contrast to the control group (0.210 ± 0.007 mm, $p < 0.001$ each) with no difference between EAO and adjuvant. The cortical surface (Ct.S, not graphically displayed) remained unaltered in EAO (10.538 ± 0.163 mm^2) compared to control (10.270 ± 0.235 mm^2, $p = 1.000$), but slightly decreased in the adjuvant group (9.530 ± 0.238 mm^2, $p < 0.05$ vs. EAO, $p = 0.087$ vs. Cont). In contrast, the cortical surface/volume ratio (Ct.S/Ct.V, **Figure 4**b) was significantly increased in EAO (18.588 ± 0.608 mm^{-1}) and adjuvant (17.594 ± 0.549 mm^{-1}) compared to control (13.670 ± 0.326 mm^{-1}, $p < 0.001$ each). Therefore, the cortical surface/volume ratio indirectly indicated a loss of cortical bone volume in EAO and adjuvant without significant differences between them. The bone mineral density (BMD, **Figure 4**c) was reduced in EAO (1.164 ± 0.010 g/cm^3, $p < 0.001$ vs. Cont 1.280 ± 0.006 g/cm^3) while adjuvant (1.270 ± 0.045 g/cm^3) showed no difference to control. Similarly, the tissue mineral density (TMD, **Figure 4**d) was decreased in the EAO group (1.480 ± 0.004 g/cm^3) compared to control (1.537 ± 0.005 g/cm^3, $p < 0.001$) and almost significantly decreased compared to the adjuvant group (1.531 ± 0.015 g/cm^3, $p = 0.053$ vs. EAO) with no difference between adjuvant and control ($p = 0.974$).

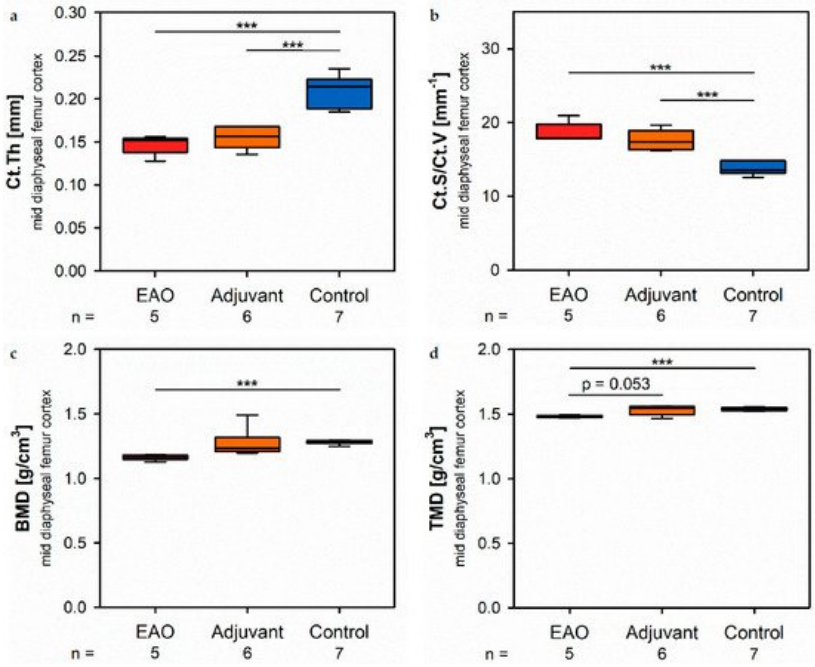

Figure 4. Microarchitecture of mid diaphyseal femur cortex in µCT. Measurement of (**a**) cortical thickness (Ct.Th), (**b**) cortical surface/volume ratio (Ct.S/Ct.V), (**c**) bone mineral density (BMD) and (**d**) tissue mineral density (TMD). Mice were immunized with testicular homogenate in adjuvant (EAO), adjuvant alone (adjuvant) or remained untreated (control). *** $p < 0.001$.

At the distal diaphysis, µCT showed a significantly thinner cortical thickness (**Figure 5**a) in the EAO (0.113 ± 0.004 mm) and adjuvant group (0.125 ± 0.005 mm) compared to the control group (0.165 ± 0.002 mm, $p < 0.001$ each) similar to the mid diaphysis. The cortical surface (not graphically displayed) remained without differences in all groups (EAO 13.012 ± 0.274 mm^2, Adj 11.556 ± 0.326 mm^2, Cont 12.686 ± 0.438 mm^2). Again, the cortical surface/volume ratio (**Figure 5**b) was significantly increased in the EAO (24.713 ± 0.982 mm^{-1}) and adjuvant group (22.396 ± 0.915 mm^{-1}) in contrast to control (17.706 ± 0.152 mm^{-1}, $p < 0.01$ each) and indicated a loss of cortical bone volume indirectly. The bone mineral density (**Figure 5**c) was reduced in EAO (0.944 ± 0.015 g/cm^3) compared to control (1.055 ± 0.005 g/cm^3, $p < 0.001$). Additionally, bone mineral density at distal diaphysis was also decreased in the adjuvant group (0.993 ± 0.020 g/cm^3, $p < 0.05$) unlike at the mid diaphysis. In contrast, the tissue mineral density (**Figure 5**d) was only reduced in the EAO group (1.273 ± 0.012 g/cm^3) compared to control (1.319 ± 0.005 g/cm^3, $p < 0.05$) while adjuvant remained unaltered (1.309 ± 0.017 g/cm^3, $p = 1.000$).

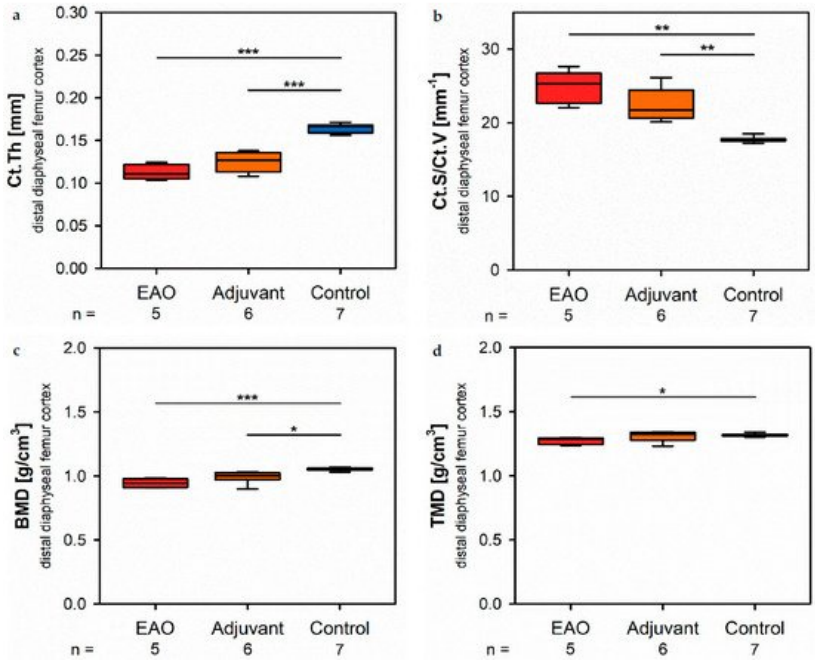

Figure 5. Microarchitecture of distal diaphyseal femur cortex in µCT. Measurement of (**a**) cortical thickness (Ct.Th), (**b**) cortical surface/volume ratio (Ct.S/Ct.V), (**c**) bone mineral density (BMD) and (**d**) tissue mineral density (TMD). Mice were immunized with testicular homogenate in adjuvant (EAO), adjuvant alone (adjuvant) or remained untreated (control). * $p < 0.05$; ** $p < 0.01$; *** $p < 0.001$.

4. Microarchitecture of Trabecular Bone

The microarchitecture of trabecular bone was studied in femora and lumbar vertebral bodies (L1) by µCT. Two-dimensional example images from µCT scans of vertebral bodies (**Figure 6**) illustrate a loss of trabecular bone mass following (a) EAO or (b) treatment with adjuvant alone compared to (c) untreated mice, similar to µCT scans of the distal femora (**Figure 3**).

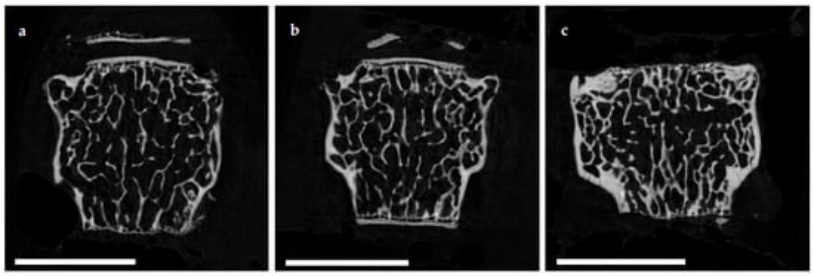

Figure 6. Two-dimensional images from µCT scans of vertebral bodies L1 (scale bar 2 mm). Mice were immunized with (**a**) testicular homogenate in adjuvant (EAO), (**b**) adjuvant alone or (**c**) remained untreated.

In the trabecular region of the femora, µCT indicated a loss of trabecular number (Tb.N, **Figure 7**a) and trabecular thickness (Tb.Th, **Figure 7**b) in EAO (Tb.N: 1.171 ± 0.099 mm^{-1}; Tb.Th: 0.038 ± 0.003 mm) and in the adjuvant group (Tb.N: 1.344 ± 0.133 mm^{-1}; Tb.Th: 0.038 ± 0.002 mm) compared to control (Tb.N: 2.771 ± 0.197 mm^{-1}, $p < 0.001$ each; Tb.Th: 0.048 ± 0.002 mm, $p < 0.05$ each). Trabecular separation (Tb.Sp, **Figure 7**c) was larger in EAO (0.276 ± 0.006 mm) and adjuvant (0.256 ± 0.005 mm) than in control (0.199 ± 0.006 mm, $p < 0.001$ each). Consequently, the bone volume fraction (BV/TV, **Figure 7**d), as well as the bone surface density (BS/TV, **Figure 7**e) were significantly decreased in EAO (BV/TV: 4.452 ± 0.447%; BS/TV: 4.427 ± 0.335 mm^{-1}) and adjuvant groups (BV/TV: 5.065 ± 0.566%; BS/TV: 5.171 ± 0.440 mm^{-1}) in comparison to control (BV/TV: 13.340 ± 1.283%, $p < 0.01$ each; BS/TV: 10.340 ± 0.698 mm^{-1}, $p < 0.001$ each). Thereby, the specific bone surface (BS/BV, **Figure 7**f) increased in the EAO (101.214 ± 6.639 mm^{-1}, $p < 0.05$ vs. Cont 79.430 ± 3.681 mm^{-1}) and adjuvant groups (103.878 ± 4.293 mm^{-1}, $p < 0.01$). This finding illustrates a pronounced loss of trabecular bone volume over trabecular bone surface. Furthermore, the structure model index (SMI; **Figure 7**g) and trabecular pattern factor (Tb.Pf, not graphically displayed) were significantly elevated in EAO (SMI: 2.252 ± 0.087; Tb.Pf: 37.822 ± 2.271 mm^{-1}) and adjuvant (SMI: 2.231 ± 0.100; Tb.Pf: 38.736 ± 2.703 mm^{-1}) compared to control (SMI: 1.699 ± 0.102, $p < 0.01$ each; Tb.Pf: 22.782 ± 2.360 mm^{-1}, $p < 0.01$ each), both indicating a degradation of trabecular integrity. The bone mineral density (BMD, **Figure 7**h) was reduced in both immunized groups (EAO 0.078 ± 0.006 g/cm^3, Adj 0.091 ± 0.008 g/cm^3) in contrast to control (0.205 ± 0.016 g/cm^3, $p < 0.001$ each) similar to the femoral cortex. Equally, the tissue mineral density (TMD, **Figure 7**i) was decreased in both immunized groups (EAO 0.922 ± 0.018 g/cm^3, Adj 0.931 ± 0.012 g/cm^3) compared to control (1.002 ± 0.012 g/cm^3, $p < 0.01$ each).

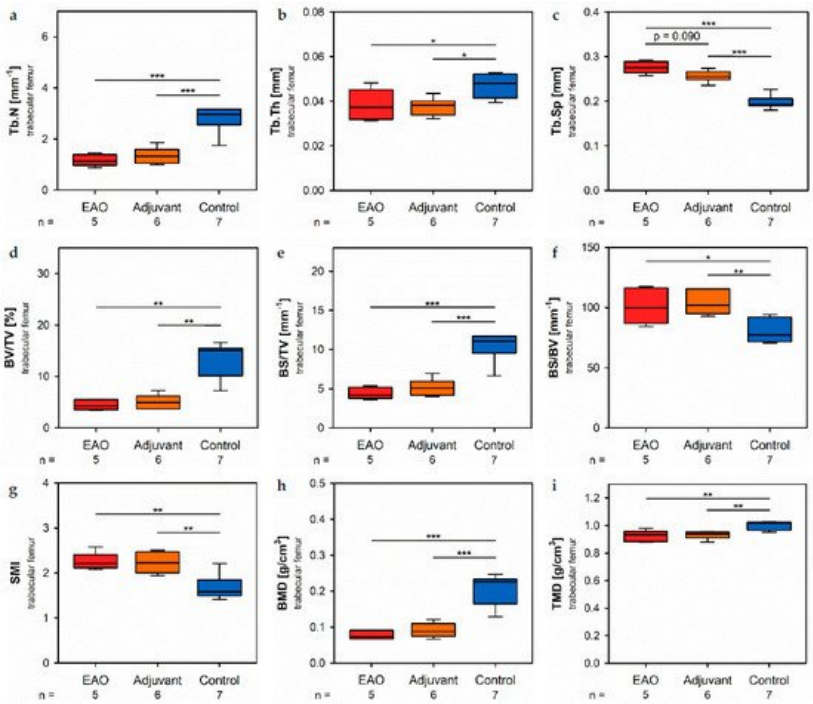

Figure 7. Microarchitecture of trabecular femur by µCT. Measurement of (**a**) trabecular number (Tb.N), (**b**) trabecular thickness (Tb.Th), (**c**) trabecular separation (Tb.Sp), (**d**) bone volume fraction (BV/TV), (**e**) bone surface density (BS/TV), (**f**) specific bone surface (BS/BV), (**g**) structure model index (SMI), (**h**) bone mineral density (BMD) and (**i**) tissue mineral density (TMD). Mice were immunized with testicular homogenate in adjuvant (EAO), adjuvant alone (adjuvant) or remained untreated (control). * $p < 0.05$; ** $p < 0.01$; *** $p < 0.001$.

Investigation of the trabecular region in vertebral bodies L1 by µCT (**Figure 8**) demonstrated generally similar alterations like the trabecular region in femora (**Figure 7**). However, several significant differences between EAO and the adjuvant group were detected in the trabecular region of vertebral bodies L1, while both groups were mostly comparable in the trabecular region of the femora.

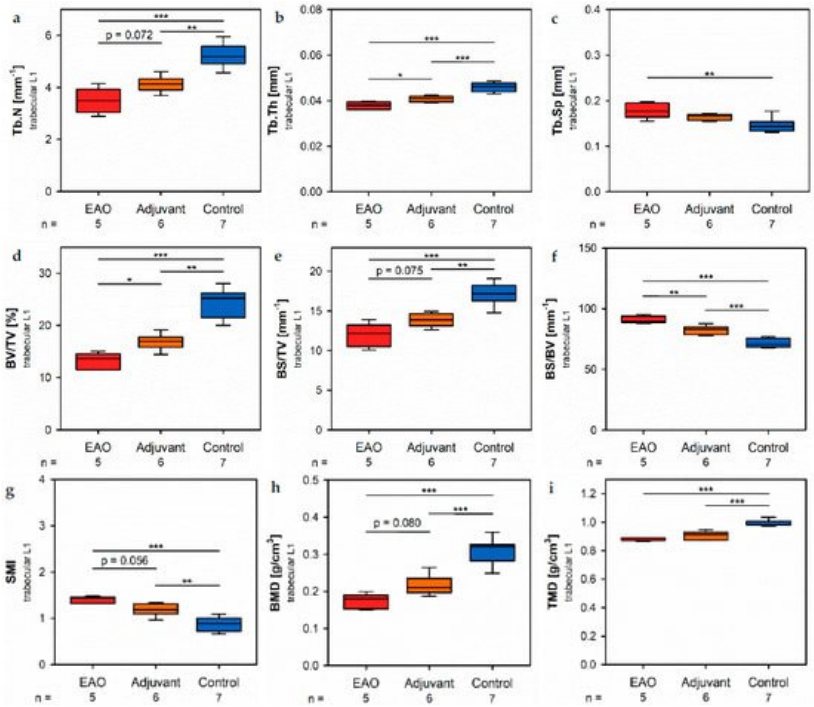

Figure 8. Microarchitecture of trabecular vertebral body L1 by µCT. Measurement of (**a**) trabecular number (Tb.N), (**b**) trabecular thickness (Tb.Th), (**c**) trabecular separation (Tb.Sp), (**d**) bone volume fraction (BV/TV), (**e**) bone surface density (BS/TV), (**f**) specific bone surface (BS/BV), (**g**) structure model index (SMI), (**h**) bone mineral density (BMD) and (**i**) tissue mineral density (TMD). Mice were immunized with testicular homogenate in adjuvant (EAO), adjuvant alone (adjuvant) or remained untreated (control). * $p < 0.05$; ** $p < 0.01$; *** $p < 0.001$.

In the vertebral bodies, L1 trabecular number (**Figure 8**a) and trabecular thickness (**Figure 8**b) were significantly decreased in the EAO (Tb.N: 3.488 ± 0.215 mm^{-1}; Tb.Th: 0.038 ± 0.001 mm) and adjuvant groups (Tb.N: 4.131 ± 0.123 mm^{-1}; Tb.Th: 0.041 ± 0.001 mm) compared to control (Tb.N: 5.243 ± 0.176 mm^{-1}, $p < 0.001$ vs. EAO, $p < 0.01$ vs. Adj; Tb.Th: 0.046 ± 0.001 mm, $p < 0.001$ each). Furthermore, trabecular number was nearly ($p = 0.072$) and trabecular thickness significantly ($p < 0.05$) lower in EAO than in the adjuvant group. The trabecular separation (**Figure 8**c) was larger following EAO (0.179 ± 0.008 mm) than in the control group (0.147 ± 0.006 mm, $p < 0.01$), but unaltered in the adjuvant group (0.164 ± 0.003 mm, $p = 0.113$). These findings resulted in a significant reduction of the bone volume fraction (**Figure 8**d) as well as the bone surface density (**Figure 8**e) in EAO (BV/TV: 13.154 ± 0.711%; BS/TV: 11.951 ± 0.659 mm^{-1}) and in the adjuvant group (BV/TV: 16.856 ± 0.628%; BS/TV: 13.868 ± 0.342 mm^{-1}) in comparison to control (BV/TV: 24.056 ± 1.132%, $p < 0.001$ vs. EAO, $p < 0.01$ vs. Adj; BS/TV: 17.149 ± 0.535 mm^{-1}, $p < 0.001$ vs. EAO, $p < 0.01$ vs. Adj). Bone volume fraction was significantly lower ($p < 0.05$), and bone surface density was almost lower ($p = 0.075$) in the EAO than in the adjuvant group. The specific bone surface (**Figure 8**f) was increased in the adjuvant group (82.504 ± 1.489 mm^{-1}, $p < 0.001$ vs. Cont 71.647 ± 1.474 mm^{-1}) and even more significantly raised after EAO (90.882 ± 1.376 mm^{-1}, $p < 0.001$ vs. Cont, $p < 0.01$ vs. Adj), again indicating a predominant loss of trabecular bone volume over trabecular bone surface. Both the structure model index (**Figure 8**g) and trabecular pattern factor (not graphically displayed) illustrated a loss of trabecular integrity in EAO (SMI: 1.400 ± 0.033; Tb.Pf: 21.194 ± 0.562 mm^{-1}) and adjuvant groups (SMI: 1.188 ± 0.054; Tb.Pf: 16.390 ± 1.011 mm^{-1}) compared to control (SMI: 0.876 ± 0.061, $p < 0.001$ vs. EAO, $p < 0.01$ vs. Adj; Tb.Pf: 10.544 ± 0.927 mm^{-1}, $p < 0.001$ vs. EAO, $p < 0.01$ vs. Adj). Again, EAO was more severely affected in this regard than the adjuvant group (SMI: $p = 0.056$; Tb.Pf: $p < 0.01$). The bone mineral density (**Figure 8**h) was decreased in both immunized groups (EAO 0.173 ± 0.009 g/cm^3, Adj 0.216 ± 0.011 g/cm^3) in contrast to control (0.308 ± 0.014 g/cm^3, p

< 0.001 each). Likewise, the tissue mineral density (**Figure 8**i) was reduced in EAO (0.883 ± 0.004 g/cm^3) and adjuvant groups (0.908 ± 0.012 g/cm^3) compared to control (0.995 ± 0.008 g/cm^3, $p < 0.001$ each).

5. Osteoblasts

Osteoblast activity was determined by the expression of alkaline phosphatase (ALP), a major enzyme of osteoblast hydroxyapatite synthesis. Enzyme histochemical staining of ALP in vertebral bodies resulted in a distinctive violet labeling located along the trabecular surface (**Figure 9**a). Histomorphometrical calculation illustrated a significantly decreased relative ALP perimeter (ALP.Pm/Tb.Pm, **Figure 9**b) in the EAO (12.720 ± 1.841%) and adjuvant groups (21.298 ± 3.237%) compared to control (43.185 ± 4.818%, $p < 0.001$ vs. EAO, $p < 0.01$ vs. Adj). This finding was supported by a reduced mRNA expression of ALP (**Figure 9**c) in the immunized groups (EAO −9.034 ± 0.102 [−ΔCP], Adj −9.017 ± 0.106 [−ΔCP]) in contrast to control (−8.461 ± 0.110 [−ΔCP], $p < 0.01$ each) determined by real-time reverse transcription polymerase chain reaction (real-time RT-PCR). Beside bone mineralization, osteoblasts are responsible for synthesis and secretion of organic bone matrix. Therefore, we examined the mRNA expression of collagen 1α1 (Col1α1, **Figure 9**d) as another parameter of osteoblast activity. Regarding the mRNA expression of collagen 1α1, we detected no significant differences between the investigated groups (EAO −2.092 ± 0.256 [−ΔCP], Adj −2.490 ± 0.082 [−ΔCP], Cont −2.411 ± 0.143 [−ΔCP]). Additionally, we conducted Von Kossa/Van Gieson staining of histological specimens, which resulted in a red labeling of osteoid (**Figure 9**f). However, the histomorphometrical calculation of relative osteoid area (O.Ar/B.Ar, **Figure 9**e) influenced neither EAO nor adjuvant compared to control (EAO 21.674 ± 1.662%, Adj 17.720 ± 4.299%, Cont 15.695 ± 3.673%).

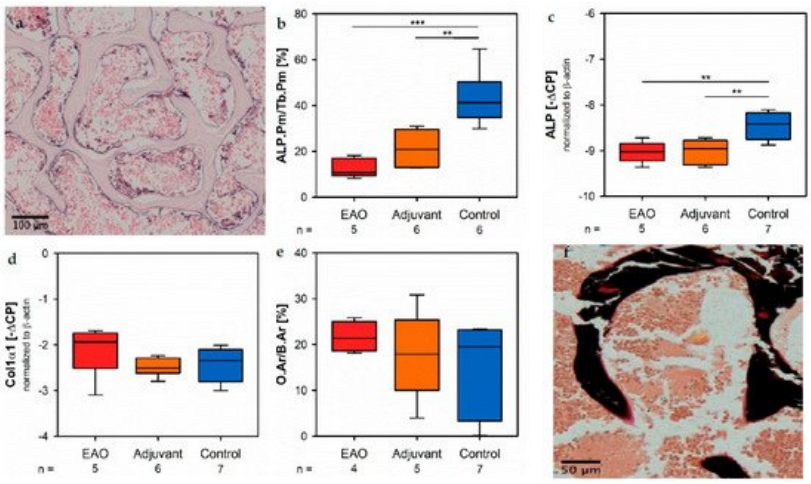

Figure 9. Osteoblasts. (**a**) Enzyme histochemical staining of alkaline phosphatase (ALP, violet) in vertebral body L3 from an untreated mouse. (**b**) Histomorphometrical calculation of relative ALP perimeter (ALP.Pm/Tb.Pm) in enzyme histochemical-stained vertebral bodies L3. mRNA expression of (**c**) ALP and (**d**) collagen 1α1 (Col1α1) in real-time RT-PCR of vertebral bodies Th10. (**e**) Histomorphometrical calculation of relative osteoid area (O.Ar/B.Ar) in vertebral bodies L2 by Von Kossa/Van Gieson staining. (**f**) Von Kossa/Van Gieson staining in vertebral body L2 from an untreated mouse (red: osteoid; black: mineralized bone; brown: bone marrow). Mice were immunized with testicular homogenate in adjuvant (EAO), adjuvant alone (adjuvant) or remained untreated (control). ** $p < 0.01$; *** $p < 0.001$.

6. Osteoclasts

Osteoclasts were identified by enzyme histochemical staining of tartrate resistant acid phosphatase (TRAP). Multinuclear, red stained cells in contact to the trabecular surface were counted as osteoclasts (**Figure 10**a). The calculation of osteoclast number in relation to trabecular perimeter (TRAP.N/Tb.Pm, **Figure 10**b) illustrated a significant reduction of osteoclasts in EAO (1.924 ± 0.488 n/mm) and adjuvant groups (1.933 ± 0.407 n/mm) compared to control (5.447 ± 0.527 n/mm, $p < 0.001$ each). These findings were supplemented by the results of real-time RT-PCR regarding cathepsin K (CtsK), another typical degrading enzyme of osteoclasts. The mRNA expression of cathepsin K (**Figure 10**c) was significantly decreased after EAO (−4.522 ± 0.292 [−ΔCP]) in comparison to control (−3.754 ± 0.159 [−ΔCP], $p < 0.05$) while it was not significantly decreased in the adjuvant group (−4.097 ± 0.129 [−ΔCP], $p = 0.620$). As a major regulatory factor of osteoclast differentiation, we determined the mRNA expression of the receptor activator of nuclear factor-kappa B ligand (RANKL, **Figure 10**d) but no significant alterations were detected (EAO −11.292 ± 0.088 [−ΔCP], Adj −11.192 ± 0.085 [−ΔCP], Cont −10.816 ± 0.237 [−ΔCP]). Additionally, we evaluated the mRNA expression of osteoprotegerin (OPG, **Figure 10**e), an inhibitor of RANKL and, thereby, regulating the differentiation of osteoclasts. Expression of osteoprotegerin was significantly reduced in the adjuvant group (−10.530 ± 0.186 [−ΔCP], $p < 0.01$ vs. Cont −9.493 ±

0.194 [−ΔCP]) and almost significantly decreased after EAO (−10.262 ± 0.249 [−ΔCP], $p = 0.062$ vs. Cont). Therefore, the reduction of osteoclast activity can neither been explained by RANKL nor by osteoprotegerin.

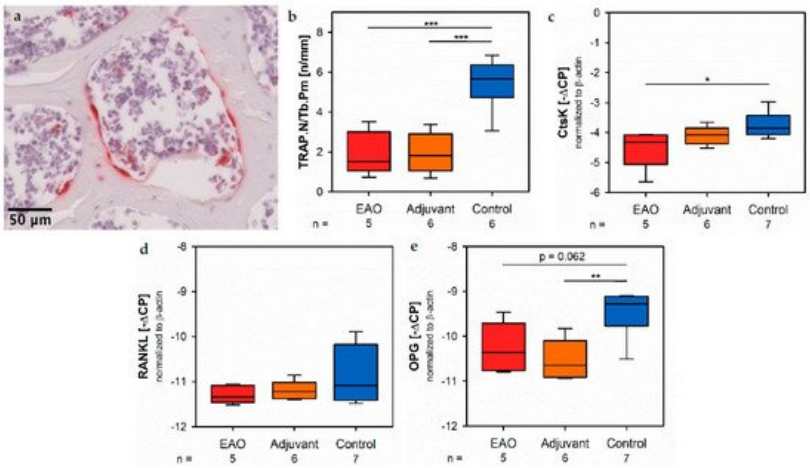

Figure 10. Osteoclasts. (**a**) Enzyme histochemical staining of tartrate resistant acid phosphatase (TRAP, red) in vertebral body L3 from an untreated mouse. (**b**) Histomorphometrical calculation of number of TRAP positive cells per trabecular perimeter (TRAP.N/Tb.Pm) in enzyme histochemical-stained vertebral bodies L3. mRNA expression of (**c**) cathepsin K (CtsK), (**d**) receptor activator of nuclear factor-kappa B ligand (RANKL) and (**e**) osteoprotegerin (OPG) in real-time RT-PCR of vertebral bodies Th10. Mice were immunized with testicular homogenate in adjuvant (EAO), adjuvant alone (adjuvant) or remained untreated (control). * $p < 0.05$; ** $p < 0.01$; *** $p < 0.001$.

7. Osteocytes and Cell-Contacts

Since sclerostin represents a typical marker of osteocytes, we analyzed the mRNA expression of the sclerostin gene (SOST, **Figure 11**a) by real-time RT-PCR. The mRNA expression of SOST was significantly decreased in both immunized groups (EAO −12.782 ± 0.277 [−ΔCP], Adj −12.522 ± 0.281 [−ΔCP]) compared to control (−11.359 ± 0.295 [−ΔCP], $p < 0.05$ each). Gap junctions link osteocytes with each other and are mandatory regarding structural integrity and cellular survival. Connexin 43 represents a characteristic element of gap junctions. The mRNA expression of connexin 43 (Cx43, **Figure 11**b) was significantly lower after EAO (−8.530 ± 0.164 [−ΔCP]) than it was in the control group (−7.759 ± 0.122 [−ΔCP], $p < 0.01$) while the adjuvant group showed an intermediate mRNA level of connexin 43 (−8.100 ± 0.097 [−ΔCP], $p = 0.199$ vs. Cont).

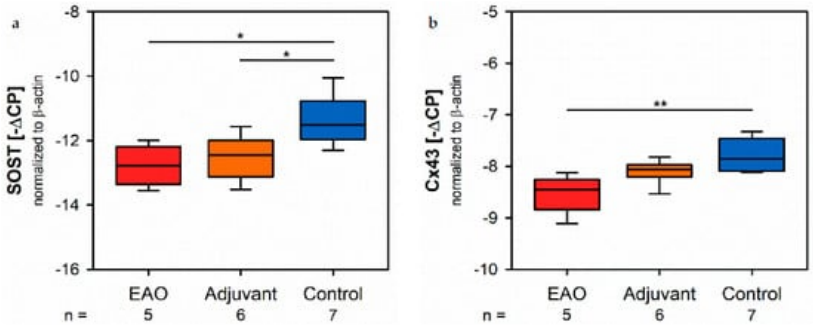

Figure 11. Osteocytes and cell-contacts. mRNA expression of (**a**) sclerostin (SOST) and (**b**) connexin 43 (Cx43) in real-time RT-PCR of vertebral bodies Th10. Mice were immunized with testicular homogenate in adjuvant (EAO), adjuvant alone (adjuvant) or remained untreated (control). * $p < 0.05$; ** $p < 0.01$.

8. Biomechanical Properties

By a three-point bending test of the femora, we objectified the consequences regarding biomechanical bone properties due to the cellular and molecular alterations following EAO described before. The maximum load (**Figure 12**a) was significantly decreased in the EAO (8.234 ± 1.099 N) and adjuvant groups (10.392 ± 1.086 N) compared to control (15.984 ± 0.665 N, $p < 0.001$ vs. EAO, $p < 0.01$ vs. Adj). The stiffness (**Figure 12**b) was significantly reduced in the EAO group (39.331 ± 7.355 N/mm, $p < 0.05$ vs. Cont 66.980 ± 4.208 N/mm) and almost significantly reduced in the adjuvant group (45.886 ± 8.284 N/mm, $p = 0.055$). Consequently, both immunized groups required less work to fracture compared to control (**Figure 12**c, EAO 4.277 ± 1.421 N/mm, Adj 5.566 ± 0.390 N/mm, Cont 12.520 ± 1.380 N/mm, $p < 0.01$ Cont vs. each).

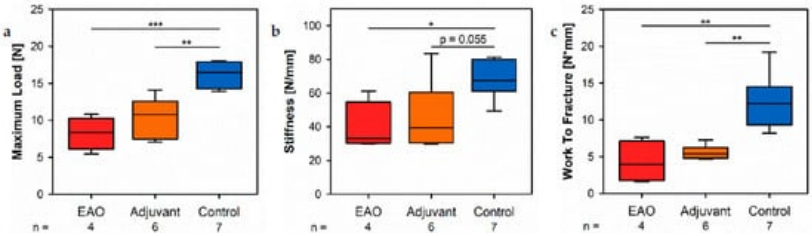

Figure 12. Biomechanical properties of the femora in the three-point bending test. Measurement of (**a**) maximum load, (**b**) stiffness and (**c**) work to fracture. Mice were immunized with testicular homogenate in adjuvant (EAO), adjuvant alone (adjuvant) or remained untreated (control). * $p < 0.05$; ** $p < 0.01$; *** $p < 0.001$.

9. Body Weight

Mice were weighed before the first immunization and 50 days after the first immunization in order to check their general health and well-being. Regarding the initial body weight (**Table 1**, Body weight before) as well as the body weight before euthanasia (**Table 1**, Body weight after) no differences between the investigated groups were noticed. Furthermore, all groups significantly gained body weight during the period of 50 days.

Table 1. Body weights before the first immunization and 50 days after the first immunization.

Parameter	Statistic	Unit	EAO (*n* = 5)	Adjuvant (*n* = 6)	Control (*n* = 7)	*p*-Values EAO vs. Adj.	EAO vs. Cont.	Adj. vs. Cont.
Body weight before								
± SEM		g	28.820 ± 1.233	27.283 ± 1.164	28.440 ± 0.680	0.978	1.000	1.000
Body weight after								
± SEM		g	30.420 ± 1.283	29.783 ± 1.262	31.540 ± 0.963	1.000	1.000	0.938
p-values	before vs. after		0.020	0.001	0.016			

References

1. Haidl, G.; Allam, J.P.; Schuppe, H.-C. Chronic epididymitis: Impact on semen parameters and therapeutic options. Andrologia 2008, 40, 92–96.
2. Schuppe, H.-C.; Meinhardt, A.; Allam, J.P.; Bergmann, M.; Weidner, W.; Haidl, G. Chronic orchitis: A neglected cause of male infertility? Andrologia 2008, 40, 84–91.
3. Schuppe, H.-C.; Pilatz, A.; Hossain, H.; Diemer, T.; Wagenlehner, F.; Weidner, W. Urogenital Infection as a Risk Factor for Male Infertility. Dtsch. Aerzteblatt Int. 2017, 114, 339–346.
4. Weidner, W.; Pilatz, A.; Diemer, T.; Schuppe, H.C.; Rusz, A.; Wagenlehner, F. Male urogenital infections: Impact of infection and inflammation on ejaculate parameters. World J. Urol. 2013, 31, 717–723.
5. Dohle, G.; Colpi, G.; Hargreave, T.; Papp, G.; Jungwirth, A.; Weidner, W. EAU Guidelines on Male Infertility. Eur. Urol. 2005, 48, 703–711.
6. Fijak, M.; Schneider, E.; Klug, J.; Bhushan, S.; Hackstein, H.; Schuler, G.; Wygrecka, M.; Gromoll, J.; Meinhardt, A. Testosterone Replacement Effectively Inhibits the Development of Experimental Autoimmune Orchitis in Rats: Evidence for a Direct Role of Testosterone on Regulatory T Cell Expansion. J. Immunol. 2011, 186, 5162–5172.
7. Nicolas, N.; Muir, J.A.; Hayward, S.; Chen, J.L.; Stanton, P.G.; Gregorevic, P.; de Kretser, D.M.; Loveland, K.L.; Bhushan, S.; Meinhardt, A.; et al. Induction of experimental autoimmune orchitis in mice: Responses to elevated circulating levels of the activin-binding protein, follistatin. Reproduction 2017, 154, 293–305.
8. Tung, K.S.; Teuscher, C. Mechanisms of autoimmune disease in the testis and ovary. Hum. Reprod. Update 1995, 1, 35–50.

9. Fijak, M.; Pilatz, A.; Hedger, M.P.; Nicolas, N.; Bhushan, S.; Michel, V.; Tung, K.S.K.; Schuppe, H.-C.; Meinhardt, A. Infectious, inflammatory and ‘autoimmune’ male factor infertility: How do rodent models inform clinical practice? Hum. Reprod. Update 2018, 24, 416–441.
10. Rucker, D.; Ezzat, S.; Diamandi, A.; Khosravi, J.; Hanley, D.A. IGF-I and testosterone levels as predictors of bone mineral density in healthy, community-dwelling men. Clin. Endocrinol. 2004, 60, 491–499.
11. Mooradian, A.D.; Morley, J.E.; Korenman, S.G. Biological actions of androgens. Endocr. Rev. 1987, 8, 1–28.
12. Clarke, B.L.; Khosla, S. Androgens and bone. Steroids 2009, 74, 296–305.
13. Francis, R.M.; Peacock, M.; Aaron, J.E.; Selby, P.L.; Taylor, G.A.; Thompson, J.; Marshall, D.H.; Horsman, A. Osteoporosis in hypogonadal men: Role of decreased plasma 1,25-dihydroxyvitamin D, calcium malabsorption, and low bone formation. Bone 1986, 7, 261–268.
14. Rozenberg, S.; Bruyère, O.; Bergmann, P.; Cavalier, E.; Gielen, E.; Goemaere, S.; Kaufman, J.M.; Lapauw, B.; Laurent, M.R.; De Schepper, J.; et al. How to manage osteoporosis before the age of 50. Maturitas 2020, 138, 14–25.
